Barishal University Journal Part 1, 5(1&2): 163-178 (2018) ISSN 2411-247X

SURFACE STRUCTURE AND REDUCTION PROCESSES OF Ti DOPED CeO_2: A ULTRA ACCELERATED QUANTUM CHEMICAL MOLECULAR DYNAMICS STUDY

Md. Khorshed Alam[1,*] Md. Alauddin[2], Rahima Nasrin[1], Md. Imran Hossain[1], Md. Saif Ishtiaque[1], M. A. Islam[1]

[1]*Department of Physics, University of Barishal, Barishal-8200, Bangladesh*
[2]*Department of Chemistry, University of Barishal, Barishal-8200, Bangladesh*

Abstract

Ti doping in CeO_2 can be used to modify its reactivity with respect to the oxygen vacancy formation and the redox properties. In the present study, we have investigated the effect of Ti doping on CeO_2 surface and its reduction properties using ultra accelerated quantum chemical molecular dynamics (UA-QCMD) method. A substitution of Ce atom by Ti atom in the surface layer causes strong structural distortion in the surface and lower oxygen vacancy formation energy compared to the undoped surface. Dopant lowers the formation energy of the active oxygen vacancy in the surface, confirming the potential for the dopant to be used in CeO_2 based materials for catalysis or solid oxide fuel cells, where the oxygen vacancy formation energy is important. It was successfully demonstrated by UA-QCMD that H_2 molecule adsorbs more strongly on the Ti doped surface compared to the undoped surface, and it is resulted in the formation of water molecule creating oxygen vacancy on the surface at 573 K.

Keywords: Ceria, Quantum chemical molecular dynamics, Ti, Hydrogen

Introduction

CeO_2 is an important catalyst in various industrial and environmental applications such as a three-way automotive exhaust catalyst (TWC) [Diwell et al.], oxygen storage [Yao et al.], oxidation of hydrocarbons, CO and decomposition of alcohol, and aldehydes. To understand the catalytic properties of both pure CeO_2 and metal/CeO_2 materials, it is imperative to examine the redox surface chemistry. It is capable of oxygen uptake and releases during excursions of the air/fuel mixture into the net oxidizing and reducing regimes, respectively. Recently, these materials have generated great interest in the solid

[*]*Correspondening author's e-mail: khorshed_du@yahoo.com*

oxide fuel cells as an alternative electrolyte for a lower temperature operation [Hibino et al.]. In the related field of "on board" hydrogen production via stream reforming of hydrocarbons, CeO_2-based catalysts are currently being considered to facilitate low temperature water gas shift-gas reaction, which convert CO and water to CO_2 and hydrogen. Most of these technological applications are based on the distinctive feature of Ce ions to easily switch oxidation states between +4 to +3.

It is generally known that one of the major deactivation pathways for TWCs is a result of shrunk the oxygen storage capacity (OSC) capabilities due to aging of the CeO_2 at high temperatures. It is therefore preferable to upgrade new CeO_2-based materials with both high redox activity (large OSC) and high thermal resistance. Many efforts regarding the improvement of the promoter performance in the three-way catalyst at high temperatures have been found that mixing with zirconium oxide immensely changes the reducibility and thermal stability of CeO_2 and demonstrated that the modified structures of CeO_2 by Ti dopant could significantly prevent the sintering of Au nanoparticles. In the $CeOx/TiO_2$ (110) systems, the Ce cations adopt a structural geometry and an oxidation state (+3) that are quite different from those seen in bulk CeO_2 or for CeO_2 nanoparticles deposited on metal substrates. Some of the oxygen in titania-doped CeO_2 is very weakly bound, with oxidation enthalpies even lower than that found with CeO_2–zirconia solutions. Although the CeO_2–titania solutions are not as stable as CeO_2–zirconia solutions, they have properties that may make them useful for some catalytic applications

Yang et al. demonstrated that the Zr dopant can enhance the adsorption of CO and also may probably promote the desorption of CO_2 molecule from the surface. They also discussed how the Zr doping changes the reduction and catalytic properties of CeO_2.

The reduction of CeO_2 and formation of oxygen vacancies have been characterized over recent years by both experiment and first principle simulations [Keating et al.]. The release and uptake of oxygen by CeO_2 allow it to participate in redox reactions, such as CO oxidation to CO_2 [Bedrane et al.] and NOx reduction. Over recent years a great deal of work has been devoted to examining how the reactivity of CeO_2 can be improved [Yang et al.]. With the example of CO oxidation, it is understand that enhancing oxygen vacancy formation is important if this formation energy can be made smaller, then oxidative power of CeO_2 will be improved and there are number of theoretical studies elaborating upon this idea, as well as experiments confirming this concept. Examples of dopants include Zr, La, Pd, Ti [Reddy et al.] and Cu.

Doping of CeO_2 with other metallic elements, such as Zr, has been shown to enhance thermal stability and to promote catalytic activity. It is believed that doping facilitates the reduction of CeO_2, by weakening the bonds to the oxygen atoms around the dopant. A number of computational studies have demonstrated that the oxygen vacancy formation

energy is lower when the surfaces is doped Zr, Pt [Nolan et al.]. Replacing a Ce atom on CeO_2 surfaces enhances CO oxidation and the Ce-O and dopant-O bonds are weakened upon formation of the doped material with reducing the oxygen vacancy formation energy and enhance the reactivity of the surface. Most of the computational studies of doped CeO_2 have investigated oxygen vacancy formation, with little work on molecular adsorption at the doped surface.

In this article, we use ultra accelerated quantum chemical molecular dynamics to study the effect of doping the (111) surface of CeO_2 with Ti on H_2 adsorption and water desorption mechanisms. Recent experimental work has focused on CeO_2 nanostructures that predominantly expose a particular surface, e.g. (111) on nanoparticle or (110) on nanorods. The earlier work has shown that the (111) surface can be made more favorable for oxygen vacancy by doping [Shapovalov et al.]. For the choice of dopant, there has been a recent experimental work related to Ti dopant in CeO_2. This dopant has formal 4+ charge, therefore it involves charge compensation or oxygen hole formation processes. This work also allows comparison with previous work on H_2 adsorption at undoped CeO_2 surface [Alam et al.] and Ti doped CeO_2 surface as well as water desorption mechanisms and provides important information on the impact of doping during the redox reactions at CeO_2 surfaces.

Computational Methods

a) Quantum Chemical Molecular Dynamics Method:

To investigate the atomic interactions between hydrogen on CeO_2 surfaces, we used our in house code UA-QCMD [Alam et al.]. The program is based on a tight-binding quantum chemistry (TBQC) calculation program "New colors" [Alam et al.] and classical molecular dynamics (MD) program "NEW RYUDO" [Elanany et al.]. In the UA-QCMD program, the center of the chemical reaction and electrons transfer dynamics are calculated by TBQC and remaining part is calculated by MD, thus realizing the study of chemical reaction and electrons transfer dynamics for a complex system.

Dynamics of atoms were carried out using the following potential functions (eq.1), which were employed to consider the ionic, covalent, and weak van der Waals interactions among atoms.

$$U = \sum_i \sum_{j>1} \left[\frac{Z_i Z_{j\,e^2}}{r_{ij}} + f_0(b_i + b_j) \exp\left(\frac{a_i + a_j - r_{ij}}{b_i + b_j} \right) - \frac{c_i c_j}{r^{\sigma}{}_{ij}} \right] + \sum_i \sum_{j>i} D_{ij} \{ \exp[-2\beta_{ij}(r_{ij} - r_0)] - 2\exp[-\beta_{ij}(r_{ij} - r_0)] \} \quad (1)$$

The first term corresponds to the Coulomb potential, and the second term corresponds to the short-range exchange repulsion potential (f_0 is the constant for unit adjustment, a is the size, and b is the stiffness), which gives a good account of the repulsive interactions arising from the overlap of electronic clouds. The third term represents van der Waals dispersive interaction (c is the constant for each atom). The fourth term in eq.(1) corresponds to the Morse-type potential, which represents covalent interactions, where D_{ij} is the bond energy, β_{ij} is the form factor, and r_0 is the bond length at minimum energy. Using these potentials determined by the above-mentioned scheme, MD simulation was performed. In this MD, a Varlet algorithm is employed to integrate equation of motion. Moreover, the temperature scaling method implemented in the system is similar to the Woodcock algorithm.

Table 1: Determined coefficient of a single ζ parameter in a Slater-type atomic orbital in eq. (3)

Element	AO	a_0	a_1	a_2	a_3	a_4	a_5
H	*s*	0.9484	1.5794	0.0000	0.0000	0.0000	0.0000
O	*s*	2.1450	0.0802	0.0185	0.0007	0.000	0.000
	p	1.9664	0.5181	1.0817	1.1475	0.000	0.000
Ti	*s*	1.1868	0.2873	-0.0664	0.0347	0.0434	0.0048
	p	1.1091	0.0085	0.0041	0.0000	-0.0013	-0.0004
	d	1.6209	0.3323	-0.0017	-0.0202	-0.0004	0.0007
Ce	*s*	2.7165	0.0332	0.0208	0.0041	0.0000	0.0000
	p	2.7165	0.0010	-0.0127	0.0093	0.0000	0.0000
	d	3.1519	0.3368	0.0000	0.0000	0.0000	0.0000
	f	4.5582	0.3363	0.0000	0.0000	0.0000	0.0000

In the TBQC, an electronic structure calculation was performed by solving the Schrödinger equation ($\boldsymbol{HC} = \varepsilon \boldsymbol{SC}$; $\boldsymbol{H}$, $\boldsymbol{C}$, ε, and $\boldsymbol{S}$ refer to the Hamiltonian matrix, eigenvectors, eigenvalues, and overlap integral matrix, respectively) with the diagonalization condition ($\boldsymbol{C^T SC} = \boldsymbol{I}$; $\boldsymbol{I}$ refers to the identity matrix). In the TBQC, the *Slater* type basis set was employed and long-range Columbic interactions were computed by the Ewald method. In order to determine the off-diagonal elements of $\boldsymbol{H}$, $\boldsymbol{H_{rs}}$, the corrected distance-dependent Wolfsberg-Helmholz formula eq. (2) was used;

$$H_{rs} = \frac{K}{2} S_{rs} \left(H_{rr} + H_{ss} \right) \qquad (2)$$

Table 2: Determined coefficient parameters of H_{rr} parameterin eq. (4)

Element	AO	b_0	b_1	b_2	b_3	b_4	b_5
H	*s*	-10.5503	-12.4348	-1.4354	0.0000	0.0000	0.0000
O	*s*	-28.6066	-15.0328	-1.4510	-0.4949	0.0419	0.0000
	p	-14.2851	-14.8159	-1.6244	0.0154	0.0434	0.0010
Ti	*s*	-7.4127	-7.1349	-0.9582	0.0364	0.000	0.0000
	p	-3.9812	-5.7018	0.0392	-0.1391	0.000	0.0000
	d	-8.0415	-7.4870	-0.6046	0.0349	0.000	0.0000
Ce	*s*	-5.5303	-5.0728	3.4414	-4.3070	1.5907	-0.1994
	p	-0.0612	-4.6247	3.8922	-4.4481	1.6406	-0.2082
	d	-8.4356	-4.8609	7.5711	-9.4497	3.5251	-0.4442
	f	-7.1929	-8.1663	3.1559	-1.5706	0.0885	0.0000

b) First-Principles Parameterisation in Tight-binding Calculation:

In order to set the Hamiltonian matrix ***H*** and overlap integral matrix ***S*** in our TBQC, exponents of a Slater-type atomic orbital (AO), denoted as ζ_r, and valence state ionization potentials (VSIPs) for the 1*s* AO of H atoms as well the 2*s* and 2*p* AOs of O atoms, 4*d* and 4*f* AOs of Ce atom sare necessary. The former parameters are used to calculate the ***S*** matrix and $\boldsymbol{H_{rs}}$ in equation (2). The latter ones are used for the diagonal element of ***H*** (H_{rr} or H_{ss}) in eq. (2). The relationship between $\boldsymbol{H_{rr}}$ and VSIP of *r*-th AO of the *i*-th atom (I^i_r) is described as $H_{rr} = -I^i_r$. In our UA-QCMD simulator, these are represented by the polynomial functions of atomic charges. The ζ_r, and H_{rr} are calculated by the polynomial functions of atomic charges described by eqs. (3) and (4), respectively.

$$\zeta_r = a_0 + \sum_{k=1}^{5} a_k \left(Z_i \right)^k \qquad (3)$$

$$H_{rr} = b_0 + \sum_{k=1}^{5} b_k \left(Z_i \right)^k \qquad (4)$$

In eqs.(3) and (4), Z_i corresponds to the atomic charge on the atom *i*. The parameters regarding ζ_r, i.e., a_0, a_1, a_2, a_3, a_4, and a_5 in eq. (3) and regarding H_{rr}, i.e., b_0, b_1, b_2, b_3, b_4, and b_5 in eq. (4), were determined so as to reproduce the binding energies and electronic structures of a H_2/CeO_2 (111) surface model obtained by DFT calculations, which are summarized in Tables 1 and 2, respectively and explained in the later section.

c) Periodic density functional theory method:

The DFT calculations were also performed in order to validate the accuracy of our TBQC method. The DMol^{3}code [Delley et al.] was used for the present purpose and double numerical basis sets with polarization functions (DNP) were employed. The parameters used in eqs. (3) and (4) were tuned comparing with DFT results (atomic charges, bond populations, atomic orbital populations and binding energies).

Table 3: Atomic charge of individual atoms obtained by DFT and TBQC.

Element	Atomic charge	
	DFT	TBQC
Ce	0.50	0.48
O	-0.25	-0.24
Ti	0.78	0.76
O	-0.39	0.38
H	0.00	0.00

The geometry optimization was performed using generalized gradient approximation (GGA) with Perdew-Burke-Ernzerhof (PBE) exchange-correlation function [Perdew et al.] was adopted for energy calculations. The charge population was analyzed by Hirshfeld method.

d) Model Preparation:

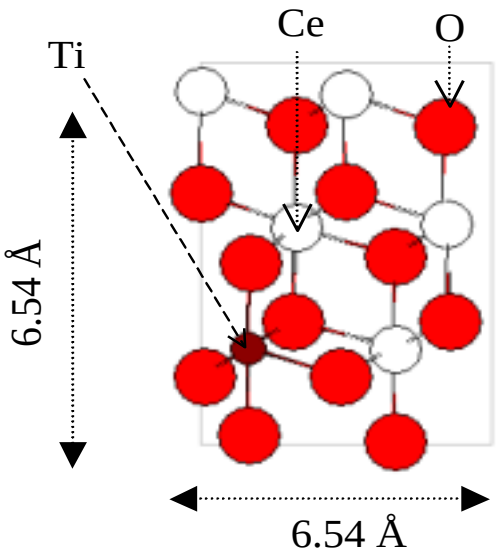

Fig.1 CeO_2 bulk model used in the validation of parameterization. Here is a white sphere represent as cerium atoms and red spheres represent as oxygen atoms.

CeO_2 is generally considered to be an ionic oxide. The (111) surface is a neutral stoichiometric plane so that no dipole moment is present upon cleaving. The slab model was 11.9 Å (twelve atomic layers) thick, with a 38.10 Å vacuum gap in the direction perpendicular to the surface. For calculations, we used a super cell that is a (3×3) expansion with 12 surface oxygen atoms, so that substitution of one surface Ce atom with the dopant gave an overall dopant concentration of 2.1% and formation of one oxygen vacancy gave a surface vacancy concentration of 8.5%, with an overall vacancy concentration of 1.04%. Upon introduction of the dopant and the vacancy, all layers except the bottom two were relaxed. H_2 molecule was adsorbed and relaxed at the doped surfaces in a number of configurations to probe the dependence of adsorption energy on the adsorption site.

Table 4: Comparison of calculated bond populations of Ce-O and H-H from DFT and TBQC.

Atomic pair	DFT	TBQC
Ce-O	0.22	0.19
H-H	0.88	0.87

Table 5: Comparison of atomic orbital population of individual species of CeO_2 bulk model and TiO_2 model calculated by DFT and TBQC

Method	Element	*s* [%]	*p* [%]	*d* [%]	*f* [%]
DFT/CASTEP	O	27.93	72.07		
	Ce	8.55	2.97	55.02	33.46
	Ti	2.94	6.61	90.44	
TBQC	O	27.92	72.07		
	Ce	8.84	2.880	54.70	33.53
	Ti	2.77	4.96	92.26	

Results and Discussion

a) Validation of parameters used in UA-QCMD:

The accuracy of the parameters used is evident in the comparison of the atomic charges, bond populations, atomic orbital populations of the CeO_2 bulk model obtained by TB-QC and DFT. In order to validate the parameters shown in Tables 1, 2 and 3. A bulk model of CeO_2 as shown in Figure 1, containing 12 Ce atoms and 24 O atoms, was prepared. The cell parameters of the CeO_2 bulk model were fixed during the calculations, which are a =7.65 Å b = 6.63 Å and c= 9.38 Å, and $\alpha=\beta= r= 90°$. Hirshfeld atomic charges, found through DFT, were compared with the atomic charges obtained by the TBQC. Atomic charges of Ce, O, Ti and H atom obtained by DFT and TBQC were close to those found with DFT as shown in Table 1.

Table 2 shows the comparison of bond population of Ce-O and H-H pairs from TBQC which are in good agreement with those from DFT. Table 3 compares the ratios of atomic orbital populations for individual atoms, where the ratios of atomic orbital populations for each valence orbital obtained by TBQC were close to those obtained by DFT.

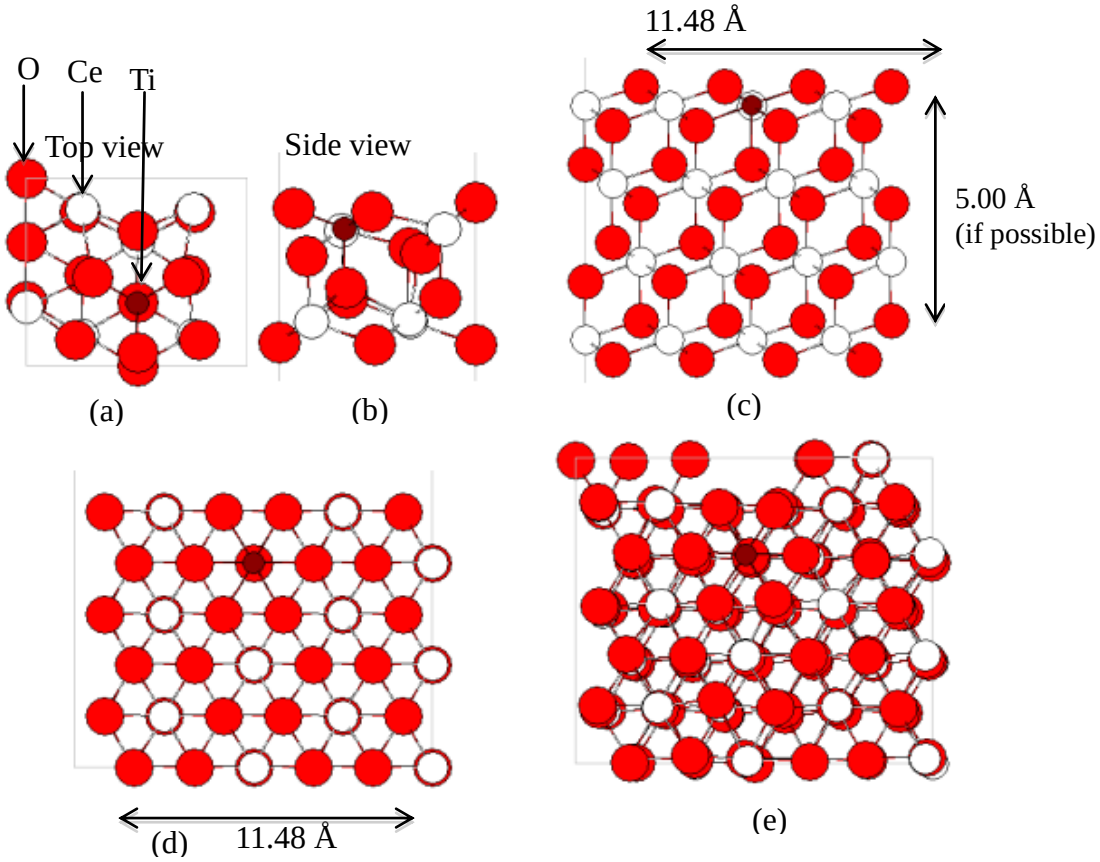

Fig. 2 Pictures of model for CeO_2 (111) surface doped with Ti. The dopant is the large gray sphere, Ce is white, and O is red. (a) Optimized structure of Ti doped CeO_2 surface (top view) (b) optimized structure of Ti doped CeO_2 surface (side view). (c) and (d) are the initial structure of Ti doped CeO_2 surface model. (e) is the surface structure after the relaxation.

b) Structure of the doped CeO_2 surfaces:

The relaxed surface structure for the doped (111) surface is shown in Figure 2 (a-e). The dopant is the gray sphere in the outermost layer in the each surface. The CeO_2 (111) surface has seven-coordinated surface Ce and three coordinated surface O, with the Ce-O distances only slightly shortened over the bulk oxide at 2.36 Å. In discussing the surface structure, the surface atoms are those in the first atomic layer that terminate the surface,

the 2nd atomic layer contains Ce and dopant, and the 3rd atomic layer contains the oxygen. Due to doping, Ti moves off its initial lattice site (Figure 2(a-e)) and surface oxygen atoms nearest the dopant are notably displaced from its lattice site. This result shows short Ti-O distances of 1.91 Å and 1.97 Å and long pair 2.14 Å and 2.12 Å, compared to the Ce-O distances of 2.36 Å in the un-doped surface. The short Ti-O distances in the surface lead to the longer pair of Ce-O distances 2.47 Å and 2.59 Å. All involve the surface Ce atom nearest the dopant.

Dopant concentration in this study is very small and therefore we would expect a smaller distortion of the coordination in the optimized structure. Due to doping, Ti moves off its initial lattice site (Figure 2(a-e)) and surface oxygen atoms nearest the dopant are notably displaced from its lattice site. This result shows short Ti-O distances of 1.91 Å and 1.97 Å and long pair 2.14 Å and 2.12 Å, compared to the Ce-O distances of 2.36 Å in the un-doped surface. The short Ti-O distances in the surface lead to the longer pair of Ce-O distances 2.47 Å and 2.59 Å. All involve the surface Ce atom nearest the dopant. Dopant concentration in this study is very small and therefore we would expect a smaller distortion of the coordination in the optimized structure. Here distortions to the surface structure in Ti doped CeO_2 are a result of the small ionic radius of Ti^{4+} (0.62 Å) compared to the Ce^{4+}(0.97 Å), and the unfavorable coordination environment in which the dopant is found.

b) The effect of Ti doping on O vacancy formation energies:

Oxygen vacancies are pertinent in the defect chemistry of CeO_2. Oxygen vacancy defect can appear on the oxide surface or in the bulk and can strongly modify the electronic and catalytic properties of the oxide. It has been found that the reducibility of CeO_2 is greatly enhanced by the dopants. We have already calculated oxygen vacancy formation energy (E_{vac}) of first layer in the surface using the eq. (5).

$$E_{vac} = E(\mathrm{TiCeO_{2vac}}) + E(1/2\mathrm{O_2}) - E(\mathrm{TiCeO_2}) \quad (5)$$

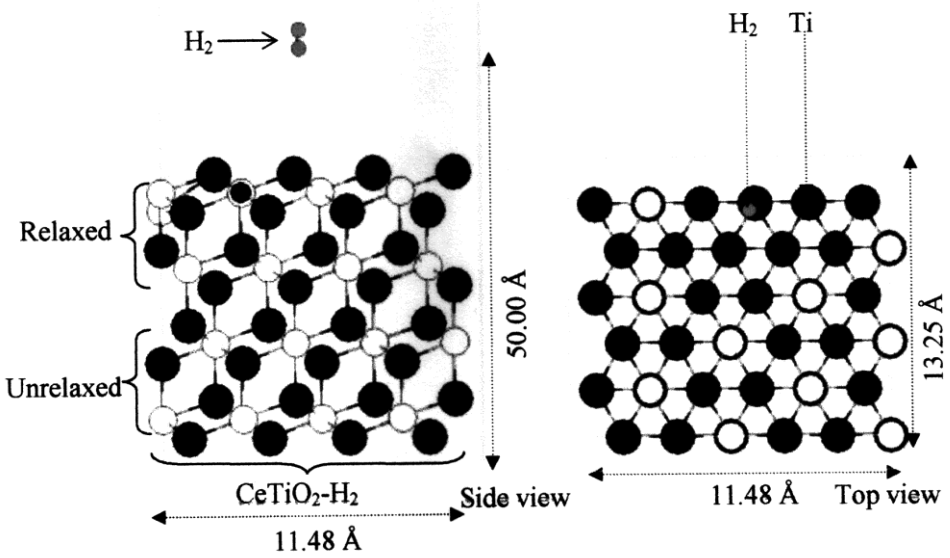

Fig. 3 Calculation model of Ti/CeO_2-H_2 system used for the UA-QCMD calculation. Left and right hand figures represent the side and top views of the model, respectively.

The formation of an oxygen vacancy near the dopant (which is the most favorable vacancy site, which is shown in Figure2). $E(TiCeO_{2vac})$ is the total energy of the slab with the vacancy, $E(TiCeO_2)$ is the total energy of the slab computed for the stoichiometric slab, and $E(1/2O_2)$ is the computed binding energy for O atom. The oxygen vacancy formation energy on the surface of CeO_2 was estimated to be -66.64 kcal/mol. For Ti doping the formation energy is smaller than that of the un-doped surface, for which the energy of forming oxygen vacancy is computed to be -89.47 kcal/mol. Thus, doping of CeO_2 surface with Ti enhances the oxidative ability of the CeO_2 surface.

d) H_2 adsorption on the doped surface:

In the calculation model in Figure 3 where the position of H_2 molecule was set at most reactive site considering adsorption energy of different sites. Here lower part of the model was un-relaxed and upper part was relaxed. The calculation temperature was 573 K and the consecutive velocity of H_2 molecule was 2700 m/s. The distance between H_2 and the top region of CeO_2 surface is equivalent to 5.56Å. During the UA-QCMD simulation a snapshot at 40 fs (Figure 6.4 (b) shows that the H_2 molecule comes approach to the surface where as a snap shot at 80 fs (Figure 4 (c) shows H_2 molecule interacts with the surface oxygen at the reactive dopant site. In the gas phase, the bond distance of H_2

was 0.74 Å and the bond information was changing while H_2 molecule was approaching to the surface. Finally, when H_2 molecule interacts with the surface, the bond length was lengthening from 0.74 Å to 0.80 Å. We investigate H_2 adsorption on the doped CeO_2 surface. We have previously studied H_2 adsorption at the un-doped CeO_2 surfaces [Alam et al.]. Here we wish to compare the details of H_2 adsorption at the doped and un-doped surfaces, because this is the fundamental interaction involved in surface reduction processes of CeO_2. The energy change upon H_2 adsorption at the surface is calculated by

$$E_{ads} = E(\mathrm{TiCeO_2}+\mathrm{H_2}) - [E(\mathrm{TiCeO_2})+E(\mathrm{H_2})] \quad (6)$$

E_{ads} is negative when the adsorbed H_2 is more stable than that in the gas phase. The adsorption energy of H_2 on the un-doped (111) surface is –28.7 kcal/mol, where as on the doped surfaces, the adsorption energy is –56.4 kcal/mol. Here the enhanced reactivity to H_2 adsorption arises because, upon adsorption on a CeO_2 surface, H_2 pulls surface oxygen atoms from the lattice site; the smaller oxygen vacancy energy, the more this process will be promoted and this results in the stabilization of the intermediate.

e) Hydrogen dissociation and water desorption:

After the adsorption,H_2 molecule dissociated homolytically on the surface and formed two OH- groups as shown in Figure 4 (e). A notable difference was found between the doped and un-doped surfaces for hydrogen adsorption and dissociation processes. The ease with which oxygen can be removed from these surfaces allows an oxygen atom to be pulled farther from the surface than for the un-doped surface. The bond lengths of two OH groups were about 1.00 Å and also bond energies were about –95 kcal/mol. There is a mutual interaction occurred between OH groups and formed water molecule creating oxygen vacancy on the surface.

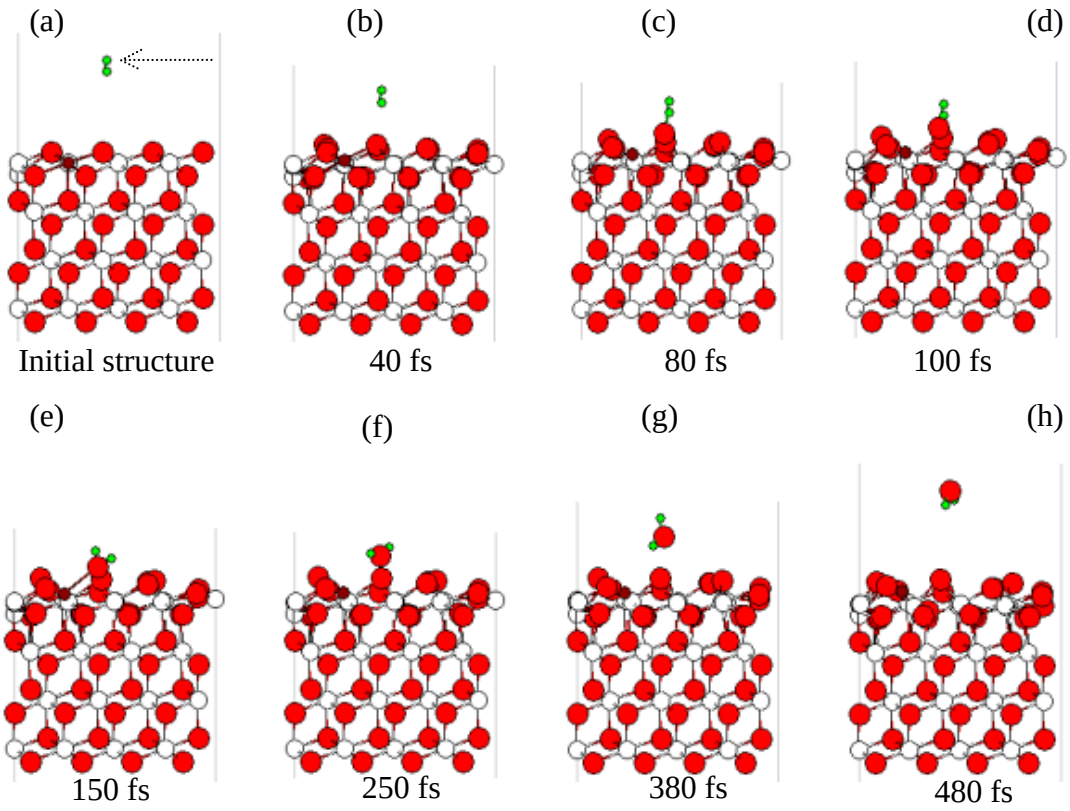

Fig. 4 Snapshot of the result from UA-QCMD calculation at different simulation steps from 0 to 480 fs: (a) Initial model of H_2/Ti/CeO_2 (b-c) the snapshots at 40 and 80 fs where H_2approaches to the surface, (d) H_2 adsorbed on the surface, (e) $H_2$was dissociated and formed OH groups, (f) is the snapshot at 250 fs where mutual interaction occurred between the OH groups. (g) shows one lattice oxygen atom about to desorbs from the surface. (h) is the snapshot at 480 fs where H_2O molecule completely desorbed from the surface.

Looking briefly at the surface, the dopant and neighboring Ce atom in the surface move apart, with the distortions in the surface and first subsurface layer that is shown in both views of the plan and the side in Figure 2. Figure 5 shows the changes of the bond length of adsorbing H_2 and the reactive surface O during the simulation. In MD simulation hydrogen approached to the reactive sites and we have considered the variation of bond lengths with respect to time. Initial distance was 5.56 Å (average) desorbed from the surface with H_2 atoms, the bond length changes to about 1.00 Å.

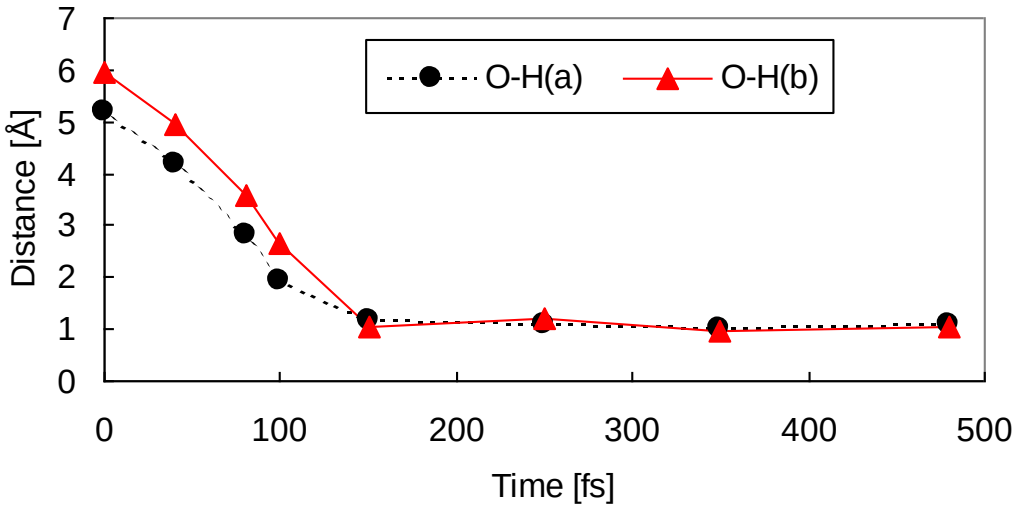

Fig. 5 Comparison of the change of the bond lengths between reactive oxygen (O) to H (a) and H (b) in H_2 during the simulation. Red solid line (triangle) indicates the change of bond length between O-H (a) and broken line (circle) indicates the change of the bond length between O to H (b).

At around 250 fs when hydrogen completely adsorbed and dissociated on the surface the O-H bonds was about 0.98 Å and finally when one atom oxygen. From the inspection it was clarified that H_2 adsorption, dissociation and desorption as a water molecule from the surface creates oxygen vacancy. The introduction of the dopant into the (111) surface of CeO_2 reduces the energy required for formation of an oxygen vacancy in the surface. The distortion of the atomic structure around the dopant site tends to weaken the Ce-O bonds and makes removal of oxygen easier. The adsorption of H_2 onto the doped surface shows the impact of the reduction of the vacancy formation energy. Comparing the adsorption energy of H_2 on the non-doped surface [Alam et al.] to the doped surface it is obvious that dopant makes the surface more reactive than that of un-doped surface.

Conclusion

In this article, based on the theoretical studies involving quantum chemical molecular dynamics, we have demonstrated the surface reduction process of Ti doped CeO_2 surface. We have analyzed the hydrogen adsorption, dissociation and water desorption mechanisms in case of Ti doped CeO_2 surface and made a comparison with the properties of the non-doped case. It was shown that Ti doping enhances the oxidative power of the

oxide, as indicating by reduction energy required for the formation of oxygen vacancy and enhanced adsorption energy of H_2.

Acknowledgements

We gratefully acknowledge to Prof. Akira Miyamoto, Tohoku Uni. Japan for his guidance and computational resources to perform this works.

References

Diwell A. F., R. R. Rajaram, H. A. Shaw and T. J. Treux. 1991. The role of ceria in three-way Catalysts, in Catalysis Automotive Pollution Control.*71 (Ed.: A. Cruq), Elsevier, Amsterdam.*

Yao H. C., Y. F. Y. Yao, 1984. Ceria in Automotive Exhaust Catalysts. *Journal of Catalysis.* **86**: 254-265.

Hibino T, A. Hashimoto, T. Inoue, J. Tokuno, S. Yoshida and M. Sano, 2000.Low-Operating Temperature Solid Oxide Fuel Cell in Hydrocarbon-Air Mixtures. *Science.* **288**: 2031-2033.

Keating, P. R. L., D. O. Scanlon and G. W. Watson. 2009. Intrinsic Ferromagnetism in $CeO_{2:}$ Dispelling the myth of vacancy site localization mediated super exchange. *Journal of Physical Condense Materials.***21**: 405-502.

Bedrane S., C. Descorme and D. Duprez. 2002. Investigation of the oxygen storage process on ceria and ceria and ceria-based. *Catalysis Today.***75**: 401-405.

Yang, Z., T. K. Woo and K. Hermansson. 2006. Effects of Zr doping on Stoichiometric and reduced Ceria: A first principle study. *Journal of Chemical Physics.***124**: 224704-9

ReddyB. M., P. Bharali, P. Saikia, A. Kahn, S. Loridant, M. Muhler and W. Gruenert. 2007. Hafnium doped ceria nano composite oxide as a novel redox addition for three-way Catalysts. *Journal of Physical Chemistry C.***111**:1878-1881.

Nolan M., V. Soto Verdugo and H. Metiu. 2008. Vacancy formation and Co adsorption on gold-doped ceria surface. *Surface Science.* **602**:2734-2742.

Shapovalov V. and H. Metiu. 2007. Catalysis by doped oxides: CO oxidation by $Au_xCe_{1-x}O_2$. *Journal of Catalysis.* **245**: 205-211.

Alam Md. K., F. Ahmed, R. Miura, A. Suzuki, H. Tsuboi, N. Hatakeyama, A. Endou, H. Takaba M. Kubo, and A. Miyamoto. 2011. Surface reduction processes of cerium

oxide surfaces by H_2 using ultra accelerated quantum chemical molecular dynamic study.*Catalysis Today*.**164:**9-15.

Alam Md. K., F. Ahmed, K. Nakamura, A. Suzuki, R. Sahnoun, H. Tsuboi, M. Koyama, N. Hatakeyama, A. Endou, H. Takaba, C. A. Del Carpio, M. Kubo and A. Miyamoto. 2009 Study of Carbon Monoxide Oxidation on CeO_2 (111) Using Ultra Accelerated Quantum Chemical Molecular Dynamics. *Journal of Physical Chemistry C*. **113**:7723-7727.

Alam Md. K., F. Ahmed, R. Miura, A. Suzuki, H. Tsuboi, N. Hatakeyama, A. Endou, H. Takaba M. Kuboand A. Miyamoto. 2010. Study of reduction processes over cerium oxide Surfaces with atomic hydrogen using ultra accelerated quantum chemical molecular Dynamics. *Applied Surface Science*. **257**:1383-1389.

Elanany M., P. Selvam, T. Yokosuka, S. Takami, M. Kubo, A. Imamura and A. Miyamoto. 2003. A quantum Molecular Dynamics Simulation Study of the initial Hydrolysis Step in Sol-Gel Process. *Journal of PhysicalChemistry B.***107**:1518-1524.

Delley B. J. 2000. From molecules to solids with the $DMol^3$ approach. *Chemical Physics.* **113**: 7756-7764.

Perdew J. P., K. Burke and M. Ernzerh of. 1996. Generalized Gradient Approximation Made Simple. *Physical Review Letters*.**77:**3865-3868.